


## Globally correlated states and control of vortex lattices in active roller fluids

Koohee Han <sup>1,2</sup>, Andreas Glatz,<sup>1,3</sup> and Alexey Snezhko<sup>1</sup>

<sup>1</sup>Materials Science Division, Argonne National Laboratory, 9700 South Cass Avenue, Lemont, Illinois 60439, USA

<sup>2</sup>Department of Chemical Engineering, Kyungpook National University, Daegu, Republic of Korea

<sup>3</sup>Department of Physics, Northern Illinois University, DeKalb, Illinois 60115, USA



(Received 31 December 2022; accepted 20 March 2023; published 19 April 2023)

Active fluids demonstrate complex collective behavior and self-organization often resulting in the emergence of localized vortices. We report on a combined experimental and computational study of the spontaneous formation of globally correlated vortex lattices formed in active roller fluids. The vortices are comprised of active ferromagnetic rollers placed on a patterned substrate promoting localization of self-organized vortices in a lattice with square symmetry. Each individual vortex spontaneously selects its chiral state (clockwise or counterclockwise). Nevertheless, confined to a square lattice, an ensemble of interacting active vortices is capable of developing correlations between chiral states of neighboring vortices. We show that such ensembles of active vortices can spontaneously evolve towards a globally correlated state with the antiferromagnetic ordering of their vorticities. We explore the correlations between chiral states of neighboring vortex pairs in response to changes in the geometry of the confining lattice. The results are supported by numerical simulations based on phenomenological coarse grained particle dynamics coupled to shallow water Navier-Stokes hydrodynamics. We show that these ordered vortex lattices formed by magnetic rollers have the ability to self-heal the antiferromagnetic order and stabilize individual vortical states in the activity regimes beyond optimal conditions for the collective vortex states. The results provide insights into the collective behavior of active magnetic roller fluids in the presence of geometrical confinement.

DOI: [10.1103/PhysRevResearch.5.023040](https://doi.org/10.1103/PhysRevResearch.5.023040)

### I. INTRODUCTION

Active colloidal materials transduce energy from the environment into mechanical motion [1–5]. The hallmark of these out-of-equilibrium systems is their natural tendency toward spontaneous formation of large-scale collective behavior [6–11]. While the majority of active colloidal matter rely on linearly translating active units, recent developments in the design of active colloids introduced systems with activities originating from spinning [12–18] facilitated by either electric or magnetic fields. Coupled to a substrate, the rotational motion of the particles results in a translational motion, which gives rise to active rollers when their direction of propulsion is not externally prescribed [12,15]. Ensembles of active rollers demonstrate a remarkable level of complex collective behavior ranging from emergence of coherent flocks, spontaneous formation of a global vortical motion under confinement [19,20], and development of a hidden structural order imprinting the dynamic state of the system [21]. In the case of active rollers powered by spontaneous Quincke rotations [22,23], modulations of the activity or chiral behavior of the rollers [24–26] lead to the emergence of multiple vortices unbound from any geometrical confinement.

Magnetic rollers energized by a uniaxial alternating magnetic field also develop spontaneous multivortical states unbound from geometrical constraints [27,28] triggered by spontaneous self-densifications in the ensemble of active magnetic rollers. While the vortices are on average long lived, they are mobile, constantly exchanging roller material with their neighbors, merging, falling apart, and spontaneously emerging in other locations. The challenge is to develop controls for the chaotic behavior of active roller systems. Tailoring an environment (e.g., hydrodynamically coupled chambers and pillars) has been successfully utilized in active bacterial suspensions to promote the formation of self-assembled vortex lattices with vorticity at each lattice site exhibiting either ferromagnetic or antiferromagnetic order [29–31]. In the case of active roller liquids, passive scatterers and obstacles have been explored as means to manipulate collective dynamics of the out-of-equilibrium ensembles [32,33].

In this paper, we report on the spontaneous formation of globally correlated vortex lattices in active magnetic rollers fluids. The formation and stability of the vortex lattices is facilitated by patterned substrates promoting a soft confinement of individual magnetic rollers in an array of circular indentations/wells arranged in vertices of a square lattice. Each well is sufficiently shallow that rollers can escape the confinement and move between the wells. Each individual well gives rise to a vortex which spontaneously selects its polar state (clockwise or counterclockwise). The reported state is dynamic by nature and exists only while energy is supplied to the system through a uniaxial alternating magnetic

Published by the American Physical Society under the terms of the [Creative Commons Attribution 4.0 International](https://creativecommons.org/licenses/by/4.0/) license. Further distribution of this work must maintain attribution to the author(s) and the published article's title, journal citation, and DOI.

field. We reveal that under certain conditions an ensemble of interacting active vortices is capable of developing correlations between chiral states of its neighboring vortices and spontaneously evolves towards a globally correlated state with antiferromagnetic ordering of their vorticities. The observed phenomenology is captured by a computational model based on phenomenological coarse grained particle dynamics coupled to shallow water Navier-Stokes hydrodynamics. Remarkably, these out-of-equilibrium vortex lattices demonstrate a self-healing behavior by an external modulation of the driving magnetic field.

## II. ACTIVE MAGNETIC ROLLERS ON A PATTERNED SUBSTRATE

To realize active vortex lattices of magnetic rollers we built on our recent discovery [28] where the emergence of multiple unconfined long-lived vortices has been attributed to spontaneous self-densifications of the rollers. Naturally, the introduction of a patterned substrate that will favor certain regions for roller densifications will provide a well-controlled breeding ground for self-assembled roller vortices.

### A. Experimental system

The patterned substrates with microwells we use here have been manufactured using a 3D printer (Prusa; Original Prusa i3 MK3S+). The 3D-printed substrates represent an array of 6-by-6 microwells with diameters of the microwells,  $D$ , ranging from 2 to 5 mm in 1 mm increment; see Fig. 1(a). The center-to-center well's separation distance,  $S$ , was also varied in the range from  $S = D$  (when the neighboring wells are in contact) to  $1.5D$ . The size of the array was selected to ensure that the magnetic field nonuniformity in the experimental setup is negligible for the observed particle dynamics. We smoothed the bottom surface of the printed wells with acetone for 15 s, air dried the templates for 10 min, and washed them with water. A well depth of 100  $\mu\text{m}$  was chosen to realize a soft confinement, such that the rollers still have the ability to travel from one well to another when energized.

A water suspension of ferromagnetic nickel (Ni) spheres (Alfa Aesar; diameter 125–150  $\mu\text{m}$ ) has been used as an active magnetic roller fluid. The detailed magnetic properties of the spherical Ni particles are provided elsewhere [34]. The experimental cell (the patterned substrate with magnetic roller fluid) is placed at the center of two magnetic coils in Helmholtz configuration. The system is energized by a vertical alternating magnetic field,  $H_z = H_0 \sin(2\pi ft)$ . Here,  $H_0$  is the field amplitude ( $H_0 = 35$  G in the experiments) and  $f$  is the field frequency. A high-speed CMOS camera (iNS1, Integrated Design Tools, Inc.) mounted on the microscope stage (Leica MZ9.5) was used to monitor the dynamics of the system at a frame rate of 50–200 frames per second. To investigate the collective dynamics of the roller ensemble, image sequences are captured and analyzed. Particle image velocity (PIV) has been performed using the MatPIV package to extract velocity fields, streamlines, and vorticity fields inside the wells. We use the vorticity to determine the polar order of each vortex and calculate the nearest-neighbor spin correlation function in

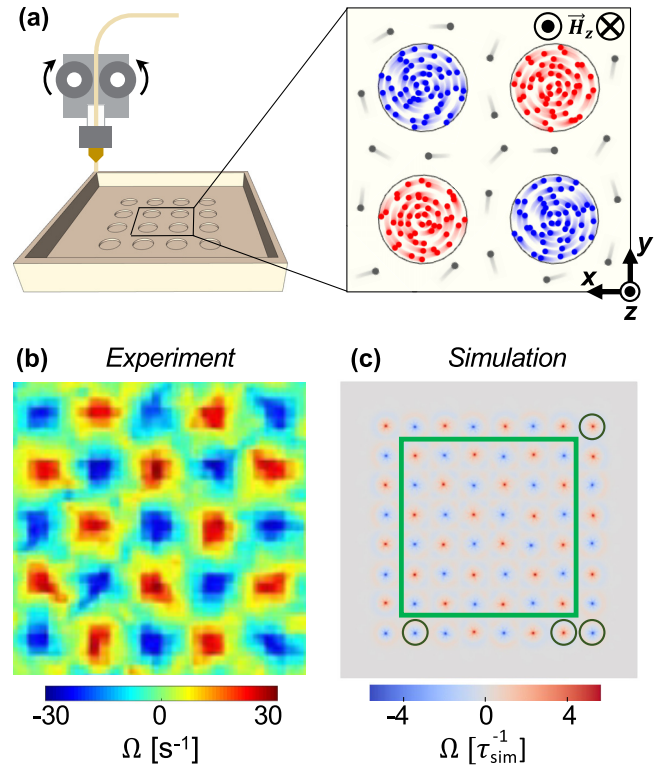


FIG. 1. Self-organized vortex lattices of active magnetic rollers on patterned substrates. (a) Schematics of the experimental system. A substrate with fabricated microwells hosts ferromagnetic Ni spheres energized by a vertical alternating magnetic field promoting a rolling motion of the spheres in the  $xy$  plane with no prescribed direction. The zoom-in view on the right illustrates the self-organization of active rollers into multivortex structures. The rollers with blue and red color compose vortical structures rotating clockwise and counterclockwise, respectively, while the ones with gray color depict rollers traveling between the wells. Panels (b) and (c) are examples of synchronized vortex lattices in experiment and simulation, respectively. In the vorticity map,  $\Omega$ , the blue and red colors correspond to the vortex structures rotating clockwise and counterclockwise, respectively. The vortex-vortex correlations lead to the antiferromagnetic ordering reflected in the alternating blue and red color of the vorticity field of the roller vorticities in the lattice. The simulated configuration shown in (c) illustrates a perfect antiferromagnetic order in the interior wells, indicated by the green square. A few disoriented vortices can be found at the perimeter, indicated by circles.

each realization of the lattice,  $C_s$ , to quantify the degree of collective synchronization and order in the system.

The spin correlation function,  $C_s$ , is defined as

$$C_s = \frac{\sum_{\langle i,j \rangle} \sigma_i \sigma_j}{\sum_{\langle i,j \rangle} |\sigma_i \sigma_j|}. \quad (1)$$

Here,  $\sigma_i$  represents the vortex polar state parameter (spin) in well  $i$ ,  $-1$  for clockwise and  $+1$  for counterclockwise vorticity, and  $\sum_{\langle i,j \rangle}$  denotes the sum over all nearest neighbor (NN) vortex pairs in the system. We extract the time evolution of a single configuration  $C_s(t)$  and sample averages of stable configurations for different initial conditions  $\langle C_s \rangle$ . For the analysis we exclude the wells at the perimeter of the array.

## B. Model and simulations

To quantify the collective dynamics observed in the system, we employ a continuum description in terms of the coarse-grained translational velocity,  $\mathbf{u} = (u_x, u_y) = \mathbf{u}(x, y, t)$ , and number density of the rollers,  $\rho = \rho(x, y, t)$ . The evolution is governed by the equation [28]

$$\partial_t \mathbf{u} = \alpha \mathbf{u} - \beta |\mathbf{u}|^2 \mathbf{u} + \mathcal{D} \nabla^2 \mathbf{u} + \frac{1}{\rho m_0} \nabla \cdot \Pi + \gamma \rho \bar{\mathbf{v}} + \boldsymbol{\Omega} \times \mathbf{u}. \quad (2)$$

Here,  $m_0$  is the mass of a roller,  $\mathcal{D}$  is the diffusivity of the particles,  $\alpha = \tau_{\text{col}}^{-1} - \tau_{\text{dif}}^{-1}$  and  $\beta = (\omega_0^2 a^2 \tau_{\text{col}})^{-1}$  are the Ginzburg-Landau coefficients that determine the transition to an ordered state and the magnitude of the order parameter [ $\tau_{\text{col}} = (2\rho a_0^2 \omega_0)^{-1}$  is the local mean collision time for spheres of radius  $a$  rolling with the angular velocity  $\omega_0 = 2\pi f$  at number density  $\rho$  and  $\tau_{\text{dif}}$  is the rotational diffusion time],  $\Pi$  is the stress tensor, and the last two terms characterize the coupling between active rollers and a passive host fluid (solvent). For more details we refer to Ref. [28]. The term  $\gamma \rho \bar{\mathbf{v}}$  is a consequence of the overdamped roller dynamics (see the Supplemental Material [35]), where  $\gamma = \frac{3}{4} \frac{a}{h} \tau_{\text{col}}^{-1}$  is a numerical prefactor.  $\bar{\mathbf{v}} = \bar{\mathbf{v}}(x, y, t)$  and  $h = h(x, y, t)$  stand for the depth-averaged in-plane velocity and the depth of the solvent, respectively. The last term,  $\boldsymbol{\Omega} \times \mathbf{u}$ , is well established in the theory of ferrofluids [36] and describes the rotation of rollers in a hydrodynamic flow with vorticity  $\boldsymbol{\Omega} = \frac{1}{2} \nabla \times \bar{\mathbf{v}}$ . In addition to these “free” equations we add a periodic confinement potential, which forces the particles (density) into the wells. The resulting force of this potential is added to the GL equation (2) for the particle velocity density. The potential is illustrated in Fig. 2(b) for a  $4 \times 4$  well geometry: each well has a flat circular region of diameter  $D$  and grows quadratically beyond that up to a distance of about 10% of the well diameter beyond which it remains constant (to avoid numerical instabilities). In the figure wells are slightly separated, i.e.,  $S > D$ , such that there is a (small) potential saddle between them. For  $S = D$ , the flat well bottoms just touch.

The hydrodynamics of the solvent is modeled for the case of a shallow solvent,  $|\nabla \mathbf{u}| \ll u/h$  and  $|\nabla \rho| \ll \rho/h$ , i.e., by the two-dimensional depth-averaged Navier-Stokes equation [37,38]

$$\partial_t \bar{\mathbf{v}} + (\bar{\mathbf{v}} \cdot \nabla) \bar{\mathbf{v}} = -g \nabla h + \nu \nabla^2 \bar{\mathbf{v}} - 3 \frac{\nu}{h^2} \bar{\mathbf{v}} + 3\pi \rho a^2 \frac{\nu}{h^2} \mathbf{u}, \quad (3)$$

where  $g$  is the gravitational acceleration and  $\nu$  the kinematic viscosity of the host fluid. The last two terms on the right-hand side originate from the no-slip condition at the rollers-solvent interface.

Lastly, we describe the dynamics of the magnetic moment density  $\boldsymbol{\mu}$  by

$$\partial_t \boldsymbol{\mu} = \alpha \boldsymbol{\mu} - \beta' |\boldsymbol{\mu}|^2 \boldsymbol{\mu} + D \nabla^2 \boldsymbol{\mu} - \epsilon \boldsymbol{\mu} \times [\boldsymbol{\mu} \times \mathbf{u}], \quad (4)$$

where, in analogy to Eq. (2),  $\alpha = \tau_{\text{col}}^{-1} - \tau_{\text{dif}}^{-1}$  and  $\beta' = (\rho^2 d_0^2 \tau_{\text{col}})^{-1}$ , with  $d_0$  being the magnetic moment of a single roller. The term  $\epsilon \boldsymbol{\mu} \times [\boldsymbol{\mu} \times \mathbf{u}]$ , which closely resembles the damping component of the Landau-Lifshitz equation for magnetization, does not affect the magnitude of  $\boldsymbol{\mu}$  but ensures its alignment along the direction of  $\mathbf{u}$  with the characteristic time  $\sim \epsilon^{-1}$ .

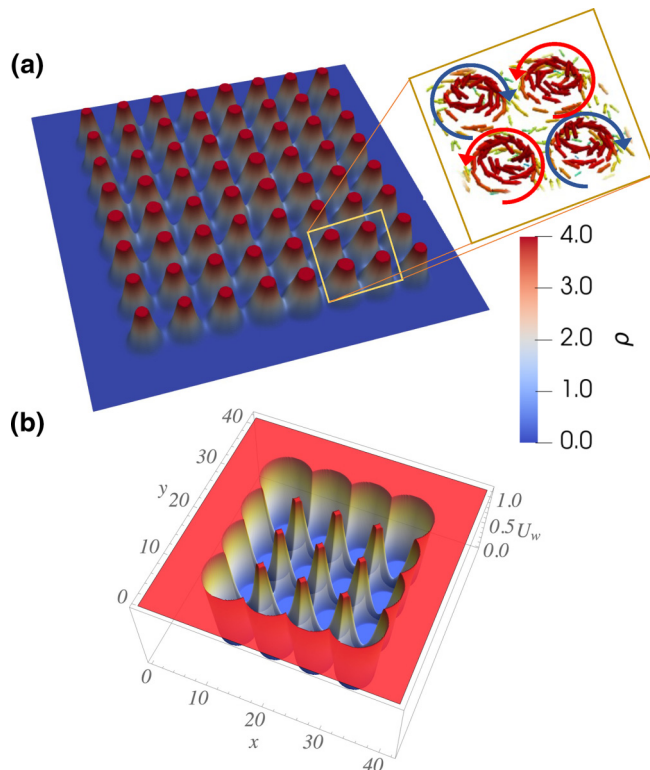


FIG. 2. Simulated system. (a) Surface plot of the particle density for the benchmark  $8 \times 8$  well system used in all simulations. The zoomed-in inset shows four wells with the particle velocities as vector plot with chirality arrows. (b) Sketch of the system’s confinement potential allowing for interaction of neighboring wells illustrated for a  $4 \times 4$  well system: the potential is flat in the center with diameter  $D$ , then increases quadratically up to a maximum. The center-to-center distance of neighboring wells is  $S$ .

Equations (2)–(4) along with the appropriate continuity conditions

$$\partial_t \rho + \nabla \cdot \rho \mathbf{u} = 0, \quad (5)$$

$$\partial_t h + \nabla \cdot h \bar{\mathbf{v}} = 0 \quad (6)$$

constitute our computational model.

*Numerical integration of the model.* We write Eqs. (2)–(6) in the dimensionless form by choosing  $\tau_{\text{dif}}$  and  $\omega_0 a \tau_{\text{dif}}$  as units of time and length, respectively. Then the velocities  $\bar{\mathbf{v}}$  and  $\mathbf{u}$  are rescaled by  $\omega_0 a$ . The roller number density is normalized by its mean value  $\bar{\rho} = \sigma / (\pi a^2)$ , where  $\sigma$  is the surface fraction of the particles. Similarly, the magnetic moment density and the host fluid depth are normalized by  $d_0 \bar{\rho}$  and  $\bar{h}$ , respectively. The frequency chosen in the simulation corresponds to the experimental frequency of 45 Hz.

The translation diffusion coefficient is given by  $D = \omega_0^2 a^2 \tau_{\text{dif}} / 4$ , as shown in [39]. We assume that the alignment of  $\mathbf{u}$  and  $\boldsymbol{\mu}$  is instantaneous and set the coefficient in front of  $\boldsymbol{\mu} \times [\boldsymbol{\mu} \times \mathbf{u}]$  in the dimensionless model to 100. To solve Eqs. (2)–(5) numerically, we discretized the system on a regular, square mesh with up to  $1024 \times 1024$  grid points. The physical size is chosen from 50 to 120 in units of  $a$  and we simulate a  $8 \times 8$  well system, where the confining well potential is tuned such that for  $S = D = 6.4$  the best order

can be achieved (see next section). A typical configuration in this system is shown in Fig. 2(a). In principle, a system with a larger number of lattice sites or a system with periodic boundary conditions can be easily implemented, though the time scale needed to reach a steady state of the vortex lattice increases with the lattice size.

All equations are integrated using quasispectral split-step methods, which calculate all second-order spatial derivatives in Fourier space. Technically, the solver is implemented on the general-purpose graphics processing units (GPU) using complex fast Fourier transforms (FFT; here the cuFFT implementation) for the  $x$  and  $y$  components of  $\mathbf{u}$ ,  $\mathbf{v}$ , and  $\boldsymbol{\mu}$  and the combined  $(h, \rho)$  vector. Compared to general-purpose CPU finite-element solvers, this method allows for an integration speed-up of three to four orders of magnitude and naturally uses periodic boundary conditions due to the FFTs. Note that the wells are not connected across the simulated system's boundaries. We typically simulate the behavior of the system for  $10^6$  time steps; each time step is  $0.004\tau_{\text{sim}}$ , where  $\tau_{\text{sim}} = f_{\text{sim}}^{-1}$  is the dimensionless time unit used in the simulations, i.e., the period of oscillation at a fixed frequency  $f_{\text{sim}}$ . For our system with  $\tau_{\text{dif}} = 0.25$  s,  $f_{\text{sim}} = 1$  corresponds to 60 Hz or  $\tau_{\text{sim}}$  to 16.7 ms, resulting in the total simulation time ( $10^6$  time steps) being about 1 min in real time. The dimensionless frequency of the external magnetic field is typically set to  $f = 0.75$  (corresponding to 45 Hz) in all simulations (for the healing protocol, the frequency is briefly lowered to 20 Hz). For the calculation of the averaged spin correlation function,  $\langle C_s \rangle$ , we ran up to 100 simulations with different random initial conditions.

### III. RESULTS AND DISCUSSION

Ferromagnetic nickel spheres develop a steady rotation in synchrony with an energizing uniaxial alternating magnetic field applied perpendicular to the substrate and display a net rolling motion in a certain range of the driving field parameters [15,40]. The particles steadily spin when the following condition is satisfied:  $\text{Im}(v[-p^2, 2q]) - p > 0$  [15]. Here the Mathieu characteristic exponent  $v$  is the function of the two parameters  $p = \alpha_r/(\omega I)$  and  $q = \mu B_0/(\omega^2 I)$ , where  $\omega = 2\pi f_B$ ,  $\eta$  is a fluid kinematic viscosity, and  $\mu$ ,  $m$ ,  $I = \frac{2}{5}mR_{\text{Ni}}^2$ , and  $\alpha_r = 8\pi\eta R_{\text{Ni}}^3$  are correspondingly the magnetic moment, mass, moment of inertia, and the rotational drag coefficient of a roller. The direction of propulsion of the individual rollers is not prescribed by the external field and is spontaneously selected by each particle. The frequency,  $f$ , of the oscillating magnetic field controls the speed of the rolling motion and is used to manipulate the activity in the system. Collective dynamics of the rollers is defined by an interplay between magnetic and hydrodynamic interactions and leads to the emergence of a set of dynamic phases ranging from gas and flocks to large scale vortices [15,20,41]. The emergence of multivortical states in magnetic roller suspensions with freestanding vortices proceeds through spontaneous local self-densifications of the rollers' number density, which give rise to free-standing self-organized vortices [27,28]. The amplitude of the external magnetic field is a convenient knob to fine-tune the balance between hydrodynamic and magnetic interactions. It was demonstrated [27] that the

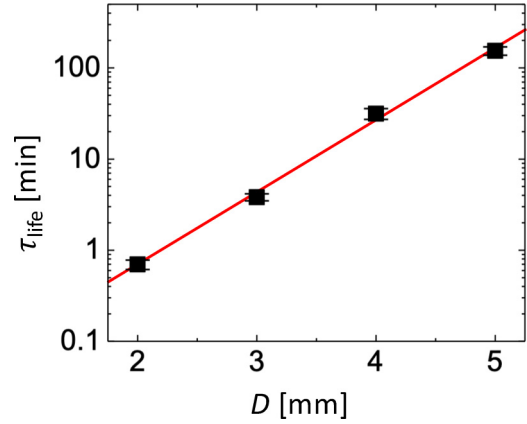


FIG. 3. Individual roller vortex lifetime,  $\tau_{\text{life}}$ , as a function of a confining well diameter,  $D$ , taken for vortices induced at  $f = 40$  Hz. The mean time of spontaneous chirality switching of vortices was used to determine the vortex lifetime. The solid line is a guide for the eye.

field amplitude can independently tune the magnetic dipole-dipole interactions between the rollers. Small variations of the field amplitude,  $H_0$ , within the range not affecting the ferromagnetic moment of the particles ( $\pm 5$  G) induce additional paramagnetic moment in the particles along the field direction and result in changes of the roller-to-roller spacing within vortices [27]. To control the location of the self-organized vortices we utilize an array of 3D-printed microwells (Fig. 1). It provides natural locations for the densifications of the rollers and effectively seeds the self-organized vortices. While the vortices on substrates without patterning are often mobile [27], the presence of patterned wells effectively localizes them and only individual rollers may still occasionally travel between the wells. When the wells are well separated, such that the interactions between individual vortices can be neglected, each individual vortex spontaneously selects its polar state (clockwise or counterclockwise) and the dynamics of the vortices is defined only by the parameters of the well confinement. For instance, as the diameter of a well decreases, the vortex inside becomes unstable and may intermittently fall apart, and self-assemble to a new vortex with a random polar state. Such behavior is reflected in a decrease of the individual vortex lifetime as the radius of the confining well decreases; see Fig. 3.

The decrease in the well separation distance promotes interactions between neighboring vortices (both by induced hydrodynamic flows and roller material exchange) and leads to a buildup of the correlations between neighboring vortical states that, eventually, results in the emergence of globally correlated vortex lattices; see Fig. 1(b) illustrating the emergence of a globally correlated vortex lattice in the experiment at  $f = 40$  Hz. A similar behavior of self-organized vortical lattices is recovered in simulations [Fig. 1(c) based on the above continuum model with confining well potentials] with alternating blue and red colors indicating the antiferromagnetic ordering of the polar states in the vortex lattices.

Naturally, the geometry of the lattice controls the dynamics of emergent vortex lattices: the degree of the correlations (or strictly speaking anticorrelations) between the polar states

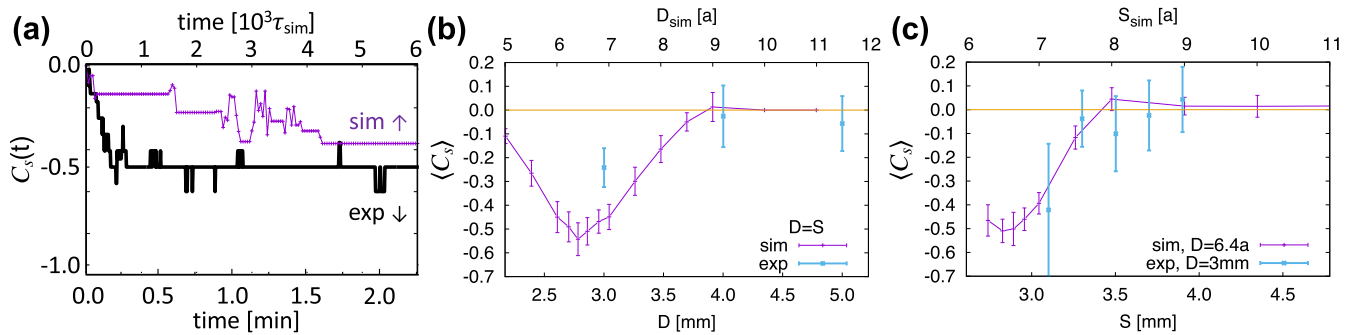


FIG. 4. Temporal and geometrical dependence of the spin correlation function. (a) Representative time evolution of the spin correlation function  $C_s(t)$  in experiment (black) and simulations (purple) starting from a random initial condition. The system typically does not reach a fully antiferromagnetic state with  $C_s = -1$  and often plateaus at  $C_s \sim -0.5$ . (See also Supplemental Movies S1, S2, and S3 [35].) The experimental curve was obtained for  $f = 40$  Hz. (b) Average spin correlation  $\langle C_s \rangle$  as function of the well diameter  $D$ . The well-to-well separation distance,  $S$ , is chosen to equal to the  $D$  (wells are in contact). Both experimental and simulation results are shown with comparable length scales. (c)  $\langle C_s \rangle$  as function of  $S$ .  $D$  is fixed at 3 mm while varying  $S$  in the experiment and  $D = 6.4a$  in the simulation [the same scaling factor as in panel (b) is used]. The numerical results in (b) and (c) are averaged over about 100 simulated configurations and show that the antiferromagnetic order is best at a certain well geometry (see text).

of the neighboring self-organized roller vortices strongly depends on the unit vortex size and vortex-to-vortex spacing, which both can be independently tuned by the well diameter,  $D$ , and the well-to-well separation distance,  $S$ .

To characterize the degree of the polar states' correlations in the vortex lattices, we calculate the spin correlation function of the lattice,  $C_s$ , where  $C_s = -1$  corresponds to a lattice with perfect antiferromagnetic ordering [Figs. 1(b) and 1(c)]. The formation of correlated polar lattices is gradual and proceeds through a slow process ( $10^3$ – $10^7$  driving field periods) of polar state switching of individual vortices that are not in a favorable polar state. Those instances of a polar state switching are manifested as steplike changes of  $C_s(t)$  shown in Fig. 4(a) (see also Supplemental Movies S1, S4 [35]). The process of a polar state reversal (and the corresponding time scale) is defined by the ability of individual vortices to change their polar state and by the influence of their neighbors (through a buildup of hydrodynamic shear stresses in the case of unfavorably oriented polar states). As illustrated in Fig. 3, the stability of a vortex (and as a result the difficulty of a polar state switching) grows with the well size. Correspondingly, when larger wells ( $D > 3.5$  mm) are brought even in close contact ( $S = D$ ), no formation of a correlated lattice is observed. On the other extreme, when the confinement is too small (a few particle diameters) the self-organized roller vortices in each well are intrinsically unstable due to a small number of rollers forming the collective vortical state, which also prevents the formation of a globally correlated vortical lattice. Figure 4(b) illustrates a typical nonmonotonic behavior of the average spin correlation function,  $\langle C_s \rangle$ , as a function of the well diameter. The experimental and computational results are shown at comparable scales (1 mm corresponds to  $2.3a$  simulation scale). It is also expected that the emergence of vortex lattices with correlated polar states will strongly depend on the interwell spacing  $S$  and vanish when  $S$  becomes large; see Fig. 4(c).

For an intermediate region of the well sizes [about 3 mm for our system as seen from Fig. 4(b)] and minimal well-to-well spacing  $S = D$  (corresponding to a lattice with the wells in contact) the system exhibits spontaneous formation

of correlated lattices with predominantly antiferromagnetic ordering of the vortical polar states; see Fig. 5 and Supplemental Movies S1, S2, and S3 [35]. Nevertheless, the system typically does not reach a perfect antiferromagnetic state with  $C_s = -1$  and often plateaus at a lower value of  $C_s$ ; see Fig. 4(a).

The onset of spin correlation in vortex lattices is observed by virtue of vortex-vortex interactions when  $S$  becomes comparable to  $D$  [Fig. 4(c)] and largely driven by macroscopic hydrodynamic flows induced by the rollers forming a vortex. Vortices in neighboring wells become entangled.

The simulation results confirm the experimentally observed behavior and provide additional insight over a wider range of well sizes and well separation distances revealing that the correlation function/antiferromagnetic (AF) order can be optimized in certain geometries. As mentioned before, the simulated  $8 \times 8$  well system was tuned to be “optimal” at a well diameter of  $D_{\text{sim}} = 6.4a$ , which translates to an optimal experimental well diameter of  $D \approx 2.7$  mm. Deviations from this optimal size result in less AF order developed over a fixed time.

The formation of vortex lattices with globally correlated polar states can be further manipulated by activity modulations (controlled by the excitation frequency,  $f$ , of the driving magnetic field) that allow one to significantly increase the “annealing” speed of the unfavorable polar states in the vortex lattice.

We note that vortex lattices formed by self-assembled roller vortices are out of equilibrium and sustain their structure only under the continuous application of a uniaxial oscillating magnetic field at certain frequencies that facilitate high roller-to-roller velocity correlations (e.g.,  $f \sim 40$  Hz) [15,40]. A modulation of the activity (by either decreasing or increasing the frequency  $f$  beyond the values favoring vortical collective states) disrupts the self-assembled vortices and promotes the formation of a gaslike phase due to a significant decrease of roller-to-roller velocity correlations [15]. Thus, intermittently switching between “gaslike” ( $f = 20$  Hz) and “vortex” ( $f = 45$  Hz) frequencies, we can temporarily disrupt and restore the

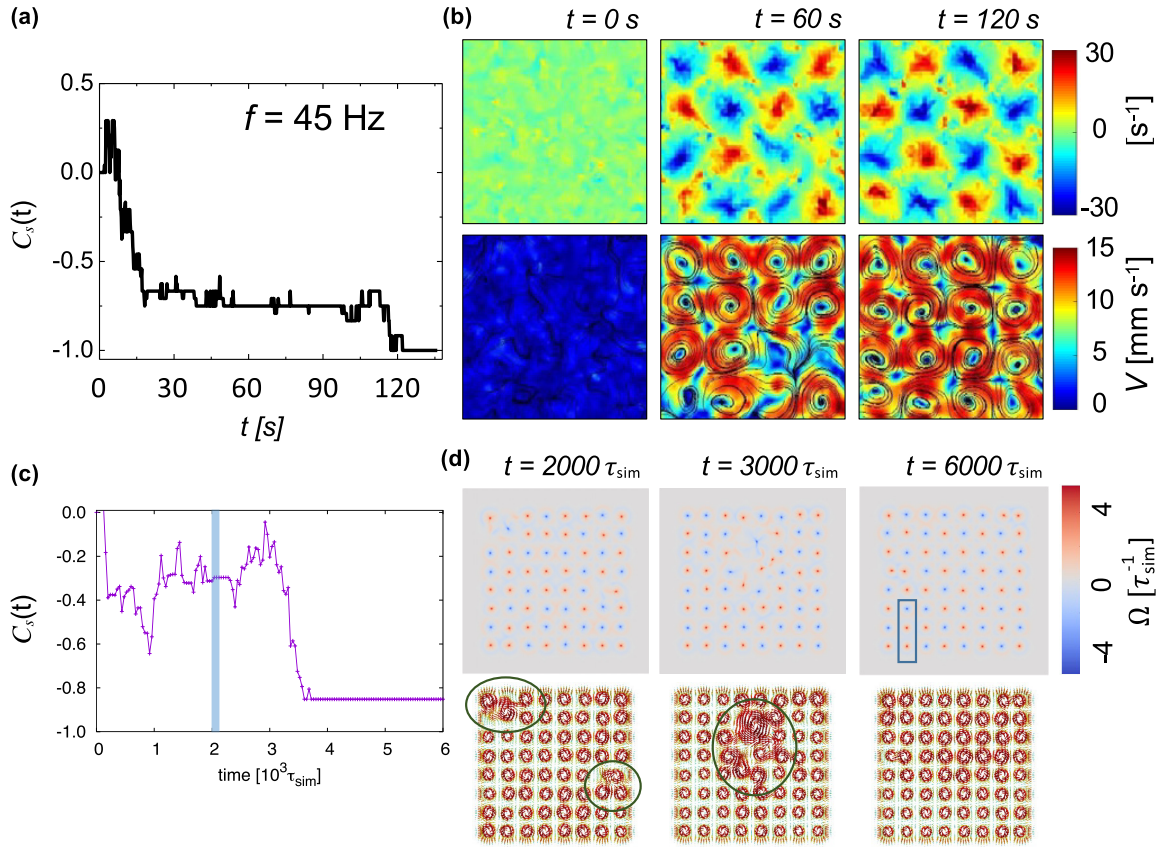


FIG. 5. Self-healing behavior in synchronized vortex lattices. (a) Time evolution of  $C_s(t)$  in a vortex lattice at a magnetic field with high  $f$  (45 Hz). At  $t = 0$ , the application of a magnetic field with  $f = 20$  Hz disrupts and resets the lattice (i.e.,  $C_s = 0$ ). As the magnetic field with  $f = 45$  Hz is applied, the vortex lattice self-heals and attains antiferromagnetic ordering (i.e.,  $\langle C_s \rangle = -1$ ). (b) Snapshots of the PIV vorticity (top) and velocity (bottom) map in the vortex lattice demonstrating the annealing process. No vortex lattice at  $t = 0$  min, an emergent vortex lattice with defects at  $t = 1$  min, and a completely ordered vortex lattice  $t = 2$  min. (c) Simulated  $C_s(t)$  for the  $8 \times 8$  well system with low frequency pulse at  $2000\tau_{\text{sim}}$  with frequency corresponding to 20 Hz. After the pulse,  $C_s$  reaches zero briefly and then drops close to the full AF state after local rearrangements shown in (d), which shows the particle density (top row) and velocity vector field (bottom row) at different times. Regions of local vortex rearrangement are indicated by ovals and disoriented vortices in the steady state after self-healing by a rectangle. (See also Supplemental Movies S5 and S6 [35].)

vortical states, making it easier for otherwise stable vortices to change their dynamic polar state to the one more favorable by the neighboring vortices. This “dynamic structure annealing” by the activity modulations is in principle analogous to thermal annealing, extensively used to help materials progress towards its equilibrium state by supplying energy to increase the rate of atom diffusion. However, there is one fundamental difference—the activity annealing of self-assembled dynamic (out-of-equilibrium) materials requires only a change in the activity (that could be increased or decreased) to break away from the dynamic state being annealed. Figure 5 illustrates the activity annealing of a square lattice of self-assembled roller vortices from an initially uncorrelated state to a globally correlated lattice with antiferromagnetically ordered polar states of the vortices. The time evolution of  $C_s(t)$  shown in Fig. 5(a) captures a rapid ( $t \sim 100$  s) descent of the structure towards the ordered state with  $C_s = -1$  [also visualized by the vorticity and velocity maps in Fig. 5(b); see Supplemental Movie S4 [35]]. A similar procedure was also realized in simulations, where we first let the system evolve at high frequency of a vortex state (corresponding to 45 Hz in the experiment), then apply a low frequency pulse (20 Hz, at simulation time

$2000\tau_{\text{sim}}$ ) and switch back to the original high frequency. Animated time evolutions are shown in Supplemental Movies S5 and S6 [35]. The result is illustrated in Fig. 5(c) with the low frequency pulse shown as a shaded vertical bar. After the pulse, the system first goes back to a disordered state and then rapidly drops to nearly ideal AF order (about three vortices remained disoriented in the interior, indicated by a rectangle in Fig. 5(d) at large times). Panel 5(d) shows the vorticity and particle velocity at different times. Examining the behavior after the low frequency pulse more closely we see that the vortex structure becomes locally dislocated from the wells (indicated by ovals in the plot), allowing the system to reassemble an AF order in a smaller subsystem (which is easier than in larger arrays).

In that sense, the activity annealing can reversibly trigger the self-healing of anti-ferromagnetic ordering in vortex lattices. The self-healing process is driven by a dynamic realignment of the polar states of adjacent vortices by macroscopic hydrodynamic flows generated by the neighbors. Stable vortices favor the nearest neighbors to have opposite chiralities of the polar states that facilitate unobstructed hydrodynamic flows in between them [27,28]. Although a

vortex lattice in the process of annealing gains rather high average spin correlation in a relatively short time, the process of a dynamic annealing of the lattice defects continues [see, for instance, Fig. 5(b) at  $t = 120$  s and Supplemental Movie S4 [35]] until the system reaches a nearly perfect antiferromagnetic ordering. Once formed, a globally correlated vortex lattice is very stable and shows no further dynamic evolution; see Figs. 5(b) and 5(c). Correlated AF vortex lattices also help to stabilize vortices that are individually unstable, for instance, while individual vortices generated at  $f = 50$  Hz are at the verge of transition to a linear flocking state [15], the antiferromagnetic lattice of vortices at  $f = 50$  Hz is stable (see Supplemental Movie S7 [35]).

#### IV. CONCLUSIONS

In summary, we report on spontaneous formation of globally correlated lattices comprised of self-assembled roller vortices in active magnetic fluid. We show how the formation and stability of such active vortex lattices is promoted by patterned substrates with predesigned soft confinements for the individual rollers. We reveal that under certain conditions (controlled by the parameters of the confining geometry) an ensemble of interacting self-organized active vortices

develops correlations between the polar states of the neighboring vortices and spontaneously evolves towards a globally correlated state with antiferromagnetic ordering of the vorticities. We introduce and demonstrate the process of “activity annealing” that allows one to significantly shorten the time scale of achieving a steady dynamic state with nearly perfect antiferromagnetic order of these out-of-equilibrium systems. The formation of globally correlated states in ensembles of emergent roller vortices facilitates the effective coupling of macroscopic hydrodynamic flows that can, in principle, be useful for directed transport applications at the microscale. Our studies provide insights into the onset of correlated motion in active magnetic roller fluids and could be extended towards more complex lattice geometries such as Lieb, Kagome, and heterogeneous lattices.

#### ACKNOWLEDGMENTS

The research was supported by the U.S. Department of Energy, Office of Science, Basic Energy Sciences, Materials Sciences and Engineering Division. The research of K.H. at Kyungpook National University was supported by the National Research Foundation of Korea grant funded by the Korea government (MSIT) No. 2022R1C1C1009769.

- 
- [1] C. Bechinger, R. Di Leonardo, H. Löwen, C. Reichardt, G. Volpe, and G. Volpe, Active particles in complex and crowded environments, *Rev. Mod. Phys.* **88**, 045006 (2016).
- [2] G. Kokot, G. V. Kolmakov, I. S. Aranson, and A. Snezhko, Dynamic self-assembly and self-organized transport of magnetic micro-swimmers, *Sci. Rep.* **7**, 14726 (2017).
- [3] M. C. Marchetti, J.-F. Joanny, S. Ramaswamy, T. B. Liverpool, J. Prost, M. Rao, and R. A. Simha, Hydrodynamics of soft active matter, *Rev. Mod. Phys.* **85**, 1143 (2013).
- [4] S. Ramaswamy, The mechanics and statistics of active matter, *Annu. Rev. Condens. Matter Phys.* **1**, 323 (2010).
- [5] A. Snezhko, Complex collective dynamics of active torque-driven colloids at interfaces, *Curr. Opin. Colloid Interface Sci.* **21**, 65 (2016).
- [6] J. Elgeti, R. G. Winkler, and G. Gompper, Physics of microswimmers-single particle motion and collective behavior: a review, *Rep. Prog. Phys.* **78**, 056601 (2015).
- [7] J. E. Martin and A. Snezhko, Driving self-assembly and emergent dynamics in colloidal suspensions by time-dependent magnetic fields, *Rep. Prog. Phys.* **76**, 126601 (2013).
- [8] T. Sanchez, D. T. Chen, S. J. DeCamp, M. Heymann, and Z. Dogic, Spontaneous motion in hierarchically assembled active matter, *Nature (London)* **491**, 431 (2012).
- [9] A. Sokolov, I. S. Aranson, J. O. Kessler, and R. E. Goldstein, Concentration Dependence of the Collective Dynamics of Swimming Bacteria, *Phys. Rev. Lett.* **98**, 158102 (2007).
- [10] T. Vicsek and A. Zafeiris, Collective motion, *Phys. Rep.* **517**, 71 (2012).
- [11] A. Zöttl and H. Stark, Emergent behavior in active colloids, *J. Phys.: Condens. Matter* **28**, 253001 (2016).
- [12] A. Bricard, J.-B. Caussin, N. Desreumaux, O. Dauchot, and D. Bartolo, Emergence of macroscopic directed motion in populations of motile colloids, *Nature (London)* **503**, 95 (2013).
- [13] M. Driscoll, B. Delmotte, M. Youssef, S. Sacanna, A. Donev, and P. Chaikin, Unstable fronts and motile structures formed by microrollers, *Nat. Phys.* **13**, 375 (2017).
- [14] K. Han, G. Kokot, S. Das, R. G. Winkler, G. Gompper, and A. Snezhko, Reconfigurable structure and tunable transport in synchronized active spinner materials, *Sci. Adv.* **6**, eaaz8535 (2020).
- [15] A. Kaiser, A. Snezhko, and I. S. Aranson, Flocking ferromagnetic colloids, *Sci. Adv.* **3**, e1601469 (2017).
- [16] G. Kokot, S. Das, R. G. Winkler, G. Gompper, I. S. Aranson, and A. Snezhko, Active turbulence in a gas of self-assembled spinners, *Proc. Natl. Acad. Sci. USA* **114**, 12870 (2017).
- [17] V. Soni, E. S. Bililign, S. Magkiriadou, S. Sacanna, D. Bartolo, M. J. Shelley, and W. Irvine, The odd free surface flows of a colloidal chiral fluid, *Nat. Phys.* **15**, 1188 (2019).
- [18] P. Tierno and A. Snezhko, Transport and assembly of magnetic surface rotors, *ChemNanoMat* **7**, 881 (2021).
- [19] A. Bricard, J.-B. Caussin, D. Das, C. Savoie, V. Chikkadi, K. Shitara, O. Chepizhko, F. Peruani, D. Saintillan, and D. Bartolo, Emergent vortices in populations of colloidal rollers, *Nat. Commun.* **6**, 7470 (2015).
- [20] G. Kokot and A. Snezhko, Manipulation of emergent vortices in swarms of magnetic rollers, *Nat. Commun.* **9**, 2344 (2018).
- [21] B. Zhang, H. Yuan, A. Sokolov, M. O. de la Cruz, and A. Snezhko, Polar state reversal in active fluids, *Nat. Phys.* **18**, 154 (2022).
- [22] G. Quincke, Ueber rotationen im constanten electrischen felde, *Ann. Phys. Chem.* **295**, 417 (1896).
- [23] A. Tsebers, Internal rotation in the hydrodynamics of weakly conducting dielectric suspensions, *Fluid Dyn.* **15**, 245 (1980).

- [24] H. Karani, G. E. Pradillo, and P. M. Vlahovska, Tuning the Random Walk of Active Colloids: From Individual Run-and-Tumble to Dynamic Clustering, *Phys. Rev. Lett.* **123**, 208002 (2019).
- [25] B. Zhang, H. Karani, P. M. Vlahovska, and A. Snezhko, Persistence length regulates emergent dynamics in active roller ensembles, *Soft Matter* **17**, 4818 (2021).
- [26] B. Zhang, A. Sokolov, and A. Snezhko, Reconfigurable emergent patterns in active chiral fluids, *Nat. Commun.* **11**, 4401 (2020).
- [27] K. Han, A. Glatz, and A. Snezhko, Emergence and dynamics of unconfined self-organised vortices in active magnetic roller liquids, *Soft Matter* **17**, 10536 (2021).
- [28] K. Han, G. Kokot, O. Tovkach, A. Glatz, I. S. Aranson, and A. Snezhko, Emergence of self-organized multivortex states in flocks of active rollers, *Proc. Natl. Acad. Sci. USA* **117**, 9706 (2020).
- [29] K. Beppu, Z. Izri, J. Gohya, K. Eto, M. Ichikawa, and Y. T. Maeda, Geometry-driven collective ordering of bacterial vortices, *Soft Matter* **13**, 5038 (2017).
- [30] D. Nishiguchi, I. S. Aranson, A. Snezhko, and A. Sokolov, Engineering bacterial vortex lattice via direct laser lithography, *Nat. Commun.* **9**, 4486 (2018).
- [31] H. Wioland, F. G. Woodhouse, J. Dunkel, and R. E. Goldstein, Ferromagnetic and antiferromagnetic order in bacterial vortex lattices, *Nat. Phys.* **12**, 341 (2016).
- [32] A. Morin, N. Desreumaux, J.-B. Caussin, and D. Bartolo, Distortion and destruction of colloidal flocks in disordered environments, *Nat. Phys.* **13**, 63 (2017).
- [33] B. Zhang, B. Hilton, C. Short, A. Souslov, and A. Snezhko, Oscillatory chiral flows in confined active fluids with obstacles, *Phys. Rev. Res.* **2**, 043225 (2020).
- [34] K. Han and A. Snezhko, Programmable chiral states in flocks of active magnetic rollers, *Lab Chip* **21**, 215 (2021).
- [35] See Supplemental Material at <http://link.aps.org/supplemental/10.1103/PhysRevResearch.5.023040> for supplemental videos.
- [36] M. Shliomis, Magnetic fluids, *Sov. Phys. Usp.* **17**, 153 (1974).
- [37] M. Belkin, A. Glatz, A. Snezhko, and I. S. Aranson, Model for dynamic self-assembled magnetic surface structures, *Phys. Rev. E* **82**, 015301(R) (2010).
- [38] A. Constantin and J. Escher, Wave breaking for nonlinear non-local shallow water equations, *Acta Math.* **181**, 229 (1998).
- [39] J. R. Howse, R. A. L. Jones, A. J. Ryan, T. Gough, R. Vafabakhsh, and R. Golestanian, Self-Motile Colloidal Particles: From Directed Propulsion to Random Walk, *Phys. Rev. Lett.* **99**, 048102 (2007).
- [40] Y. Wang, S. Canic, G. Kokot, A. Snezhko, and I. Aranson, Quantifying hydrodynamic collective states of magnetic colloidal spinners and rollers, *Phys. Rev. Fluids* **4**, 013701 (2019).
- [41] G. Kokot, A. Vilfan, A. Glatz, and A. Snezhko, Diffusive ferromagnetic roller gas, *Soft Matter* **15**, 3612 (2019).